# THE STAR FORMATION NEWSLETTER

## No. 343 21-26

2021. 8. 18　泉奈都子（ASIAA）

21. Characterization of dense Plank clumps observed with Hershel and SCUBA-2

22. A major asymmetric ice trap in a planet-forming disk: I. Formaldehyde and methanol

23. A stellar mass dependence of structured disks: a possible link with exoplanet demographics

24. Spectral index of synchrotron emission: insight from the diffuse and magnetized interstellar medium

25. Molecular line signatures of cloud-cloud collisions

26. Understanding the angular momentum evolution of T Tauri and Herbig Ae/Be stars

# 22. A major asymmetric ice trap in a planet-forming disk: I. Formaldehyde and methanol

Van der Marel et al.

Oph IRS 48のダストトラップにおけるcomplex organic chemistryの研究

- Target: Oph IRS48
  - The Herbig disk　(d~135 pc)
  - ダストトラップの典型的な例であると知られている
  - 先行研究により$H_2CO$が検出されているが、$CH_3OH$は検出されていない（上限値のみ）

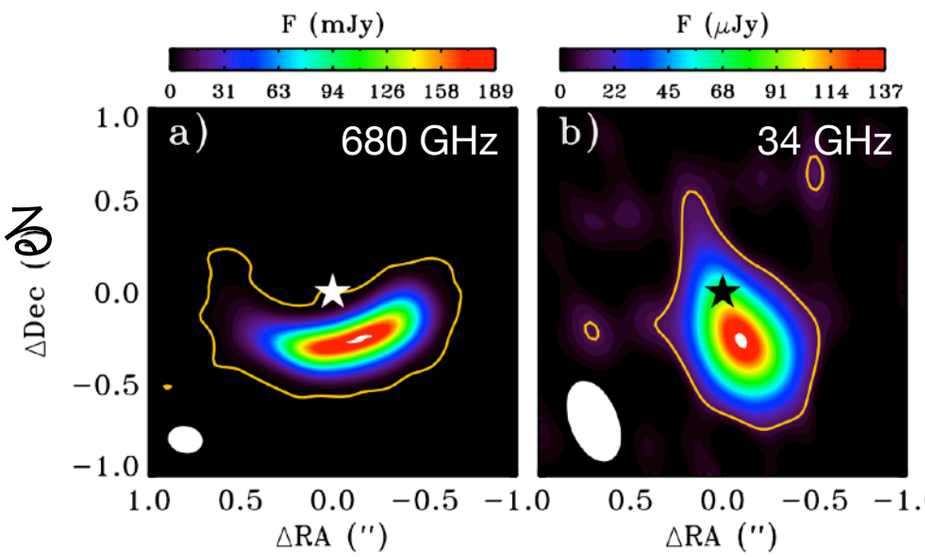


Van der Marel et al. 2015

- Observation data and results
  - ALMA Band 7 in polarization mode (Cycle 5)
  - 7つの$H_2CO$輝線、6つの$CH_3OH$輝線が検出

| Molecule | Transition | Rest frequency (GHz) | $E_u$ (K) | $g_u$ | log $A_{ul}$ | $F_{int}$ (mJy km s$^{-1}$) |
|---|---|---|---|---|---|---|
| o-$H_2CO$ | $5_{1,5}$-$4_{1,4}$ | 351.768648 | 62 | 33 | -2.92013 | 836 |
| o-$H_2CO$ | $5_{3,3}$-$4_{3,2}$ | 364.275141 | 158 | 33 | -3.05097 | 391 |
| o-$H_2CO$ | $5_{3,2}$-$4_{3,1}$ | 364.288914 | 158 | 33 | -3.05065 | 574 |
| p-$H_2CO$ | $5_{0,5}$-$4_{0,4}$ | 362.736024 | 52 | 11 | -2.86264 | 577 |
| p-$H_2CO$ | $5_{2,4}$-$4_{2,3}$ | 363.945876 | 100 | 11 | -2.93377 | 377 |
| p-$H_2CO$ | $5_{4,2}$-$4_{4,1}$/$5_{4,1}$-$4_{4,0}$[a] | 364.103257 | 241 | 11 | -3.30139 | 99 |
| a-$CH_3OH$ | $14_{1,13}$-$14_{0,14}$ | 349.106997 | 260 | 116 | -3.35603 | 198 |
| a-$CH_3OH$ | $1_{1,1}$-$0_{0,0}$ | 350.905100 | 17 | 12 | -3.47949 | 89 |
| e-$CH_3OH$ | $4_{0,4}$-$3_{-1,3}$ | 350.687651 | 36 | 36 | -4.06195 | 215 |
| e-$CH_3OH$ | $7_{-2,6}$-$6_{-1,5}$ | 363.739868 | 87 | 60 | -3.76767 | 141 |
| e-$CH_3OH$ | $8_{1,7}$-$7_{2,5}$ | 361.852195 | 105 | 68 | -4.11248 | 125 |
| e-$CH_3OH$ | $11_{0,11}$-$10_{1,9}$ | 360.848946 | 166 | 92 | -3.91831 | 155 |

[a] Lines are blended.

Rest frequencies and other properties are taken from CDMS: $E_u$ is the upper energy level, $g_u$ the degeneracy and $A_{ul}$ the Einstein $A$-coefficient.

- Results

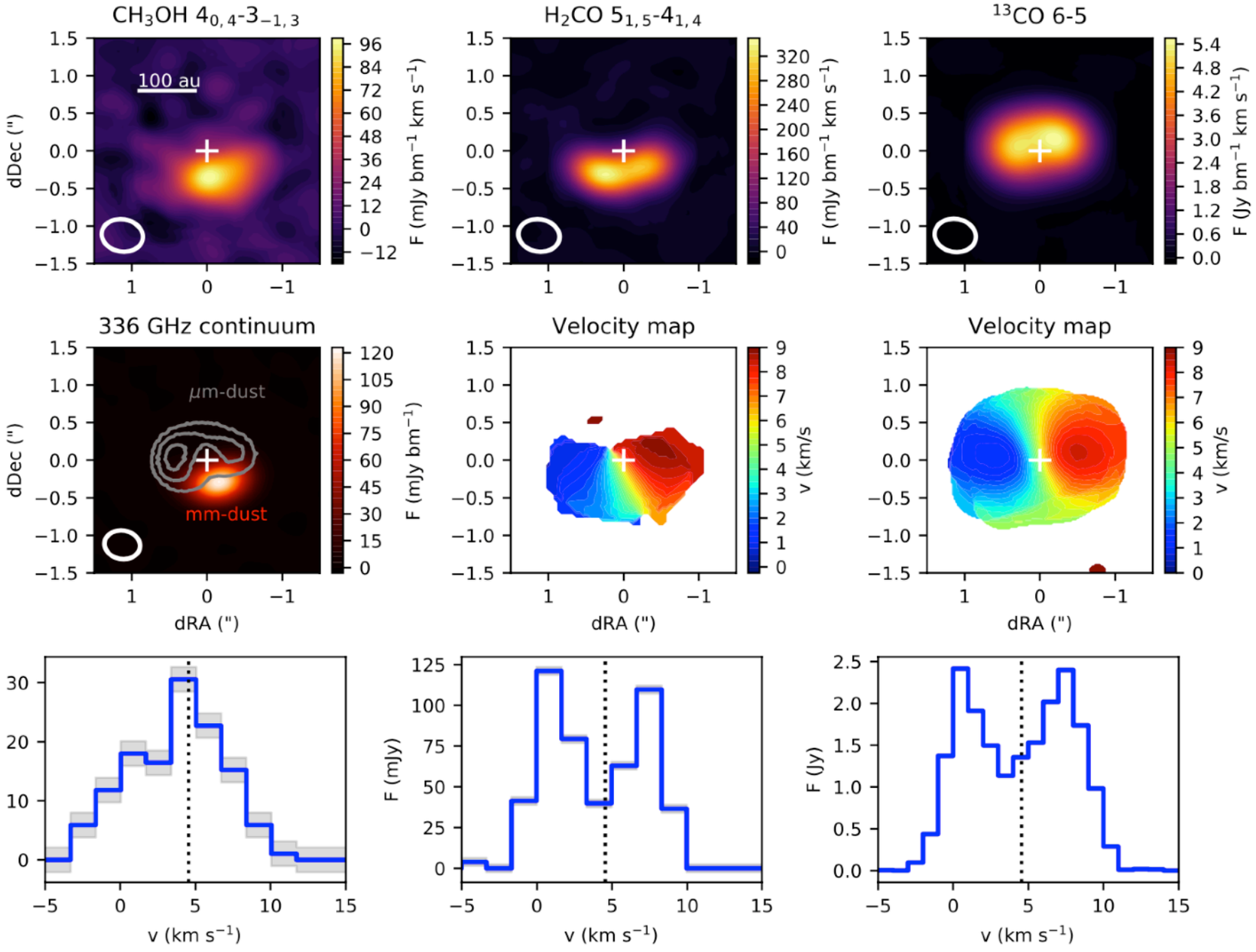


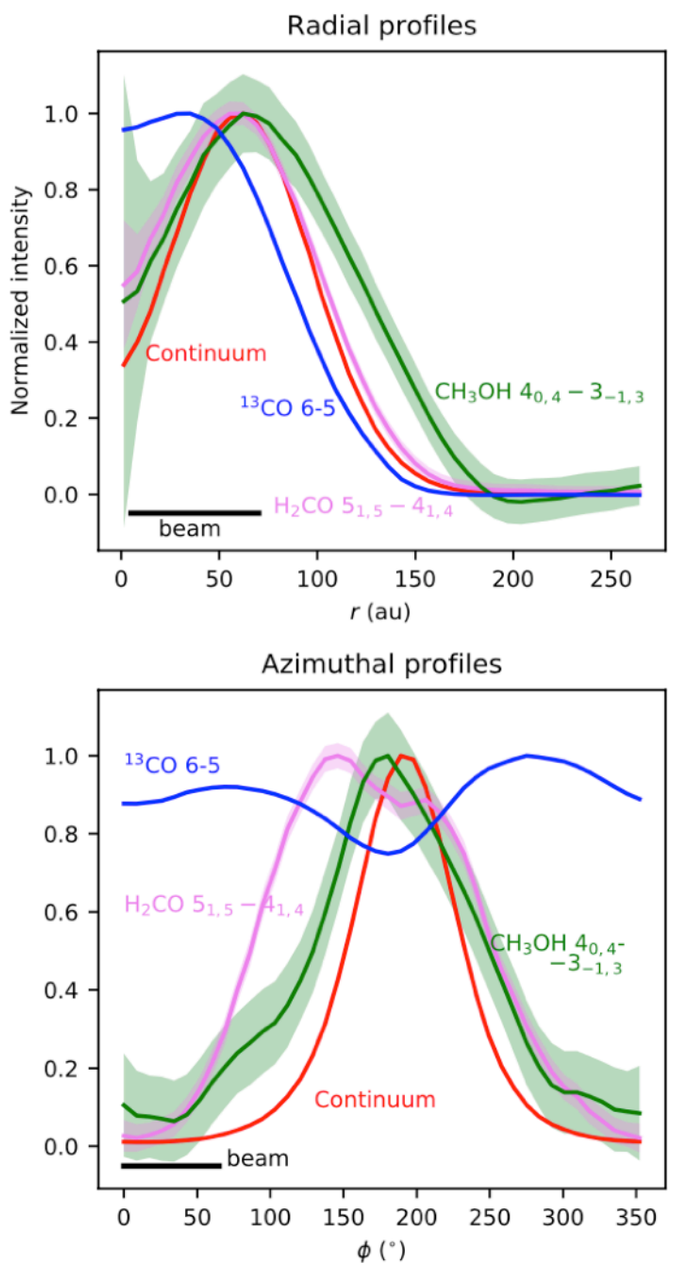


**Fig. 1.** Overview of the brightest $H_2CO$ and $CH_3OH$ lines using Briggs weighting, the 336 GHz continuum and the $^{13}CO$ 6-5 map with a similar beam size for comparison. The top row shows the zero-moment maps, the middle row the continuum and the first moment maps and the bottom row the disk integrated spectra. The $\mu$m-sized grain distribution as traced by 19 $\mu$m VISIR data (Geers et al. 2007) is indicated in the continuum image. The source velocity is indicated by a vertical dotted line. The grey shades indicate the noise levels in the spectra.

**Fig. 2.** Radially and azimuthally averaged profiles of the brightest $H_2CO$ and $CH_3OH$ lines from the Briggs weighted images, combined with the profiles from $^{13}CO$ 6-5 and the 355 GHz continuum imaged at the same beam size of 0.55×0.44".

- Discussion
  - Herbig diskではCOM (Complex organic molecules)は形成されないと予想されていた (due to their warmer midplane )
  - $H_2CO/CH_3OH$ ~ 0.2 → ice chemistry が主な形成メカニズム
  - Excitation temperature > 100 K → disk midplane (~ 70 K) からの放射ではない

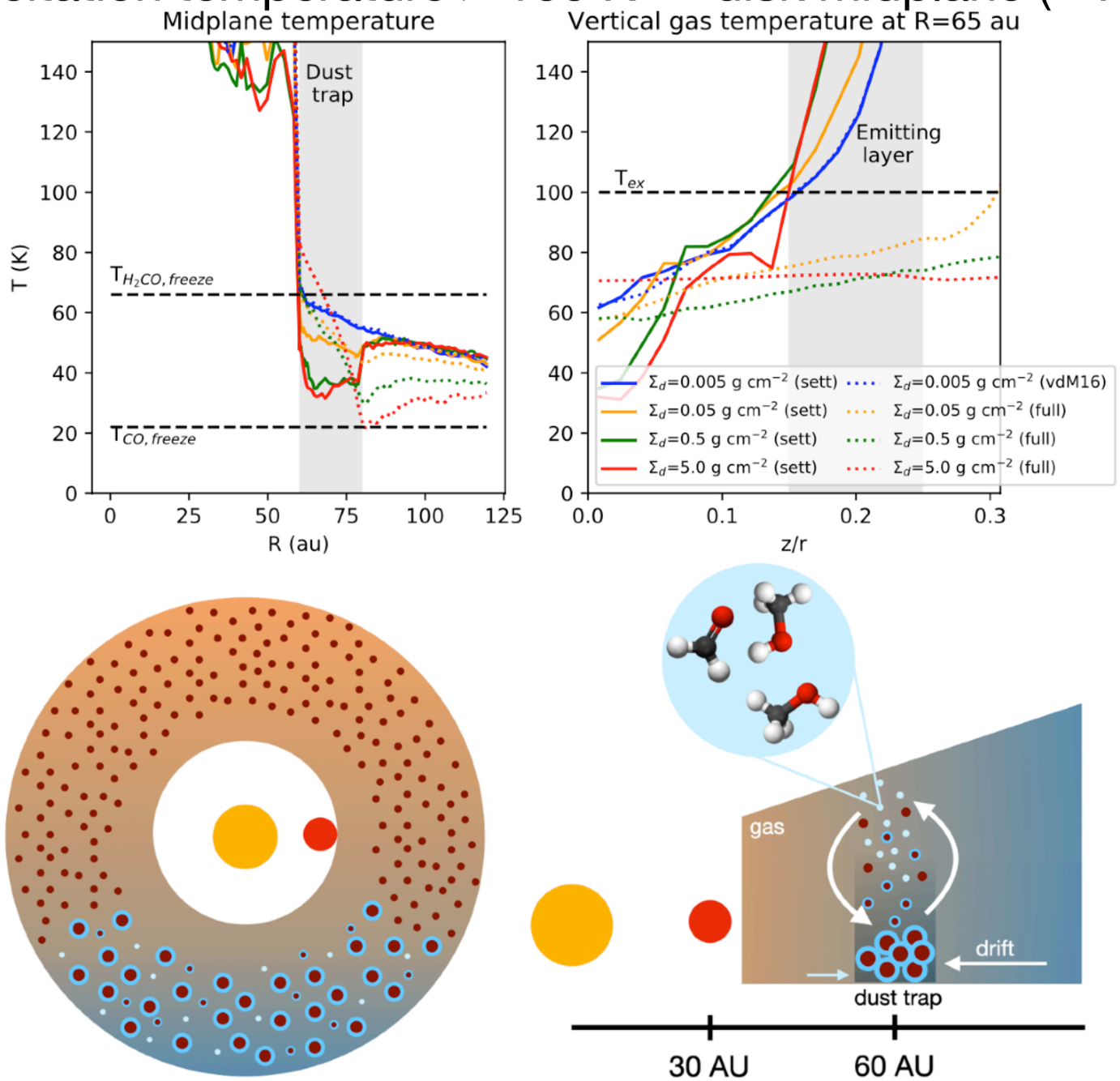


**Fig. 4. Top left:** Radial dust temperature profiles of the midplane. **Top right:** Vertical gas temperature profiles at 65 au, just inside the dust trap. Both temperature profiles are based on our physical-chemical DALI models with different dust surface densities (Figure C.1, C.2). In the midplane, the gas temperature is equal to the dust temperature. The plots demonstrate that the dust trap provides sufficiently low temperatures for a COM ice reservoir in the settled midplane, whereas the temperatures in the emitting layer are sufficiently high to explain the derived excitation temperatures. **Bottom:** Sketch of the proposed scenario for the complex organic chemistry in a dust trap based on this work. The blue-orange gradient indicates the predicted temperature structure in the disk the large arrows the vertical and radial transport of the icy pebbles, and the small arrow the thermal desorption at the inner edge of the dust trap

- ダストトラップ内のダスト(dust-to-gas ratio: > 1)がUVを遮蔽し、ダストとガスの温度を下げる
- 円盤内部の効率的な垂直輸送が必要であり、それは乱流によって説明可能
- IRS 48はCOMの放射とダストトラップに明確な関連性を検出した初の例である

# 25. Molecular line signatures of cloud-cloud collision

Priestley and Whitworth

Cloud-Cloud collisionを示すトレーサーとして、HCN,NH3が衝突時にどのように観測されるか検証した

- Collision を示すと言われているBridging feature (CO観測で検出されている)

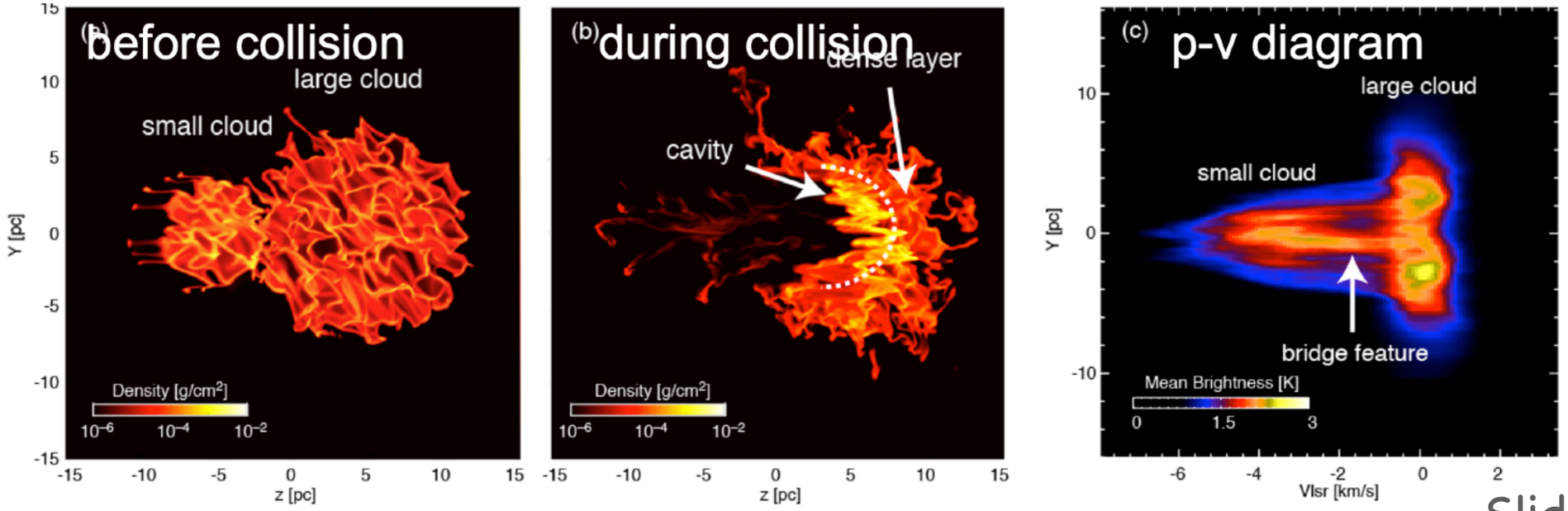


Slide by Torii-san

- COだと衝突ではなくたまたま視線速度上に雲が重なってBridge構造のように見える可能性もある

  → 高密度ガストレーサーであるHCN, NH3についても Hydrodynamical simulations, time-dependent chemistry, radiative transferを組み合わせて検証

- Method
  - Simulation: PHANTOM, a smoothed-particle hydrodynamics code
  - $R_{\rm large} = 5\,{\rm pc},\ M_{\rm large} = 10^4\,{\rm M}_\odot,\ \rho_{\rm large} = 1.3\times10^{-21}\,{\rm g\,cm^{-3}};\ n_{\rm large} = 280\,{\rm H_2\,cm^{-3}}$
    $R_{\rm small} = 2.5\,{\rm pc},\ M_{\rm small} = 2.5\times10^3\,{\rm M}_\odot,\ \rho_{\rm small} = 2.6\times10^{-21}\,{\rm g\,cm^{-3}}\quad n_{\rm small} = 560\,{\rm H_2\,cm^{-3}}$

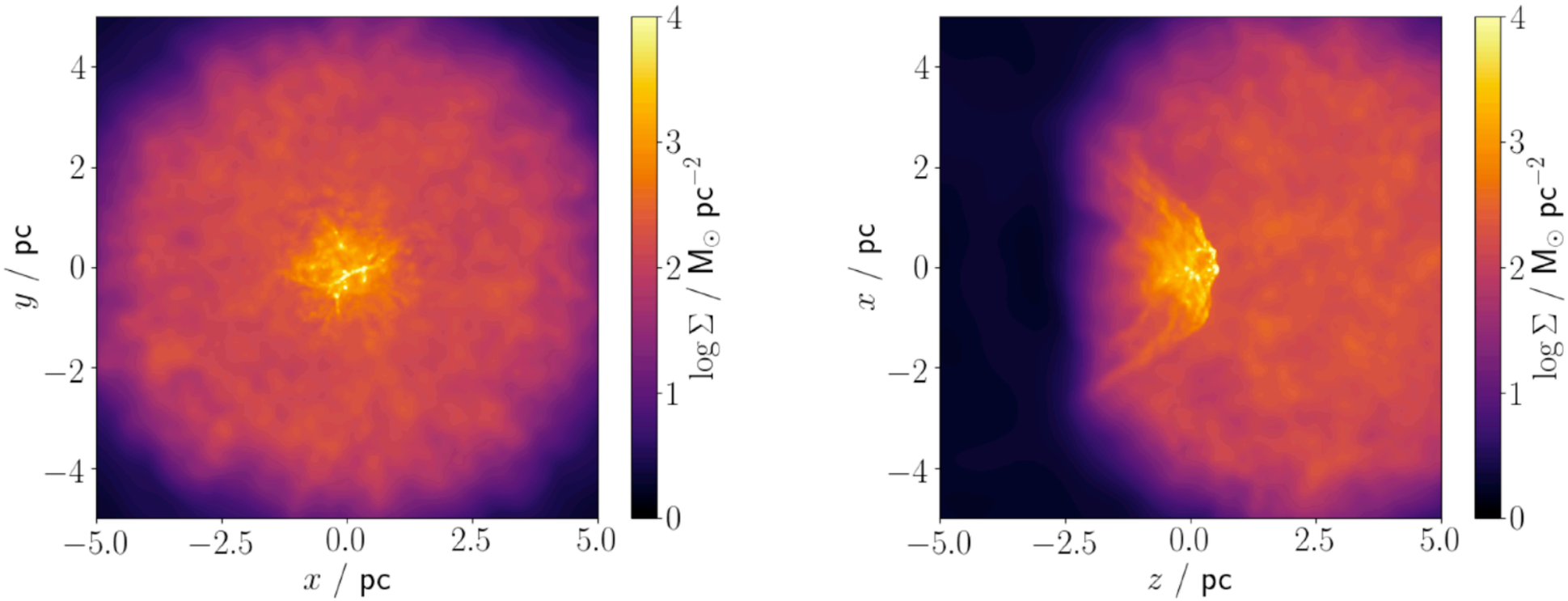


**Figure 1.** Surface density maps from the cloud-collision simulation at $t_{\rm end} = 0.49\,{\rm Myr}$. *Left panel:* looking along the collision axis, i.e. projected on the $z=0$ plane. *Right panel:* looking perpendicular to the collision axis, i.e. projected on the $y=0$ plane.

これと比較するために、独立に進化した雲がたまたま視線速度上に重なるモデル（Chance-alignment, $v_{\rm large} = v_{\rm small} = v_{\rm col} = 0$ km/s）についても検証した

- Results

Collision

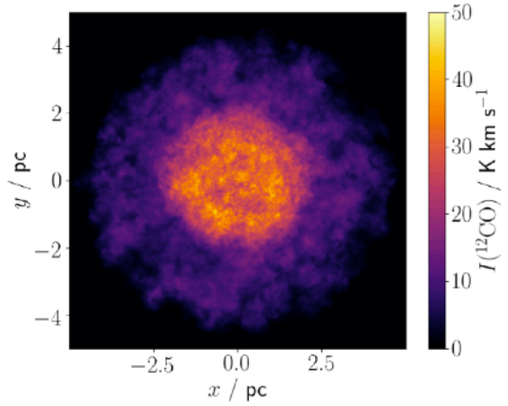


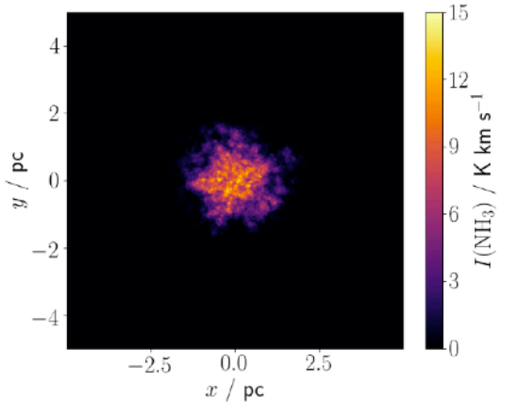


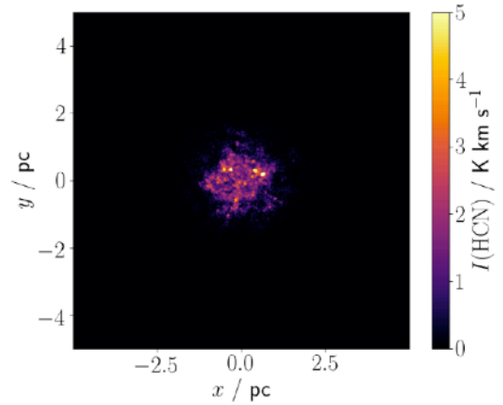











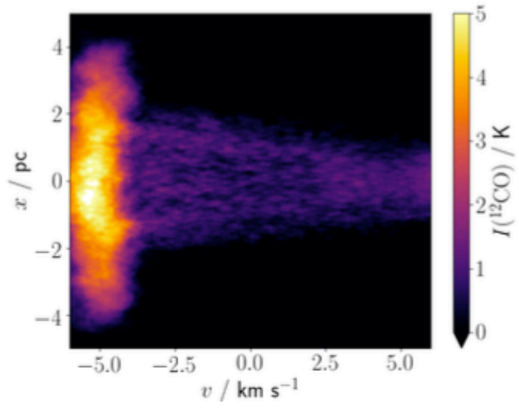


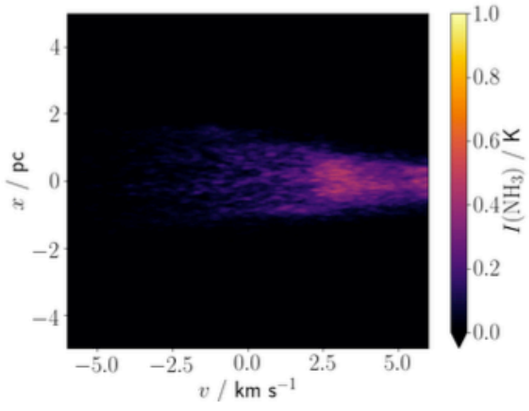


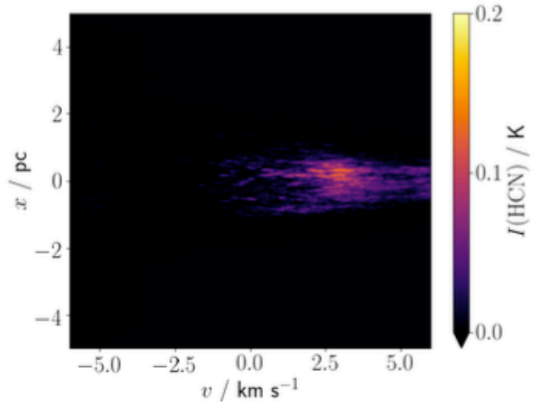


Chance-alignment

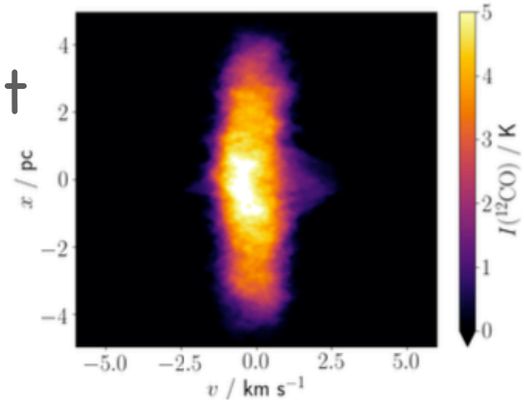


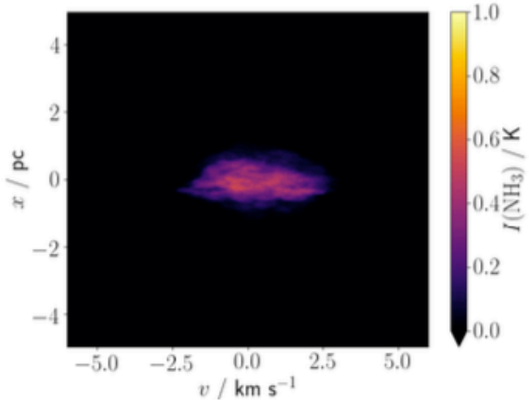


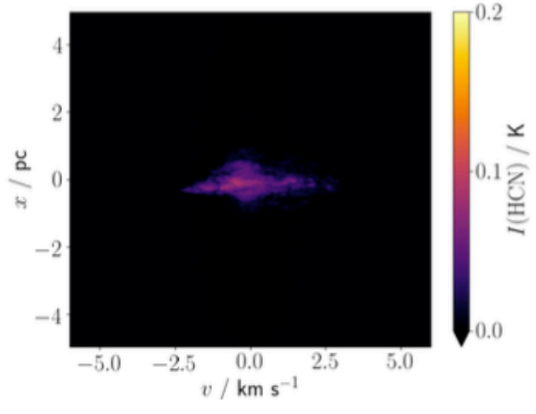


Collisionの場合、$NH_3$,HCNはショックによって圧縮された領域のみをトレースしているのに対し、

Chance-alignmentの場合はCO, $NH_3$, HCNは同様の速度構造を示している

- Results

Collision

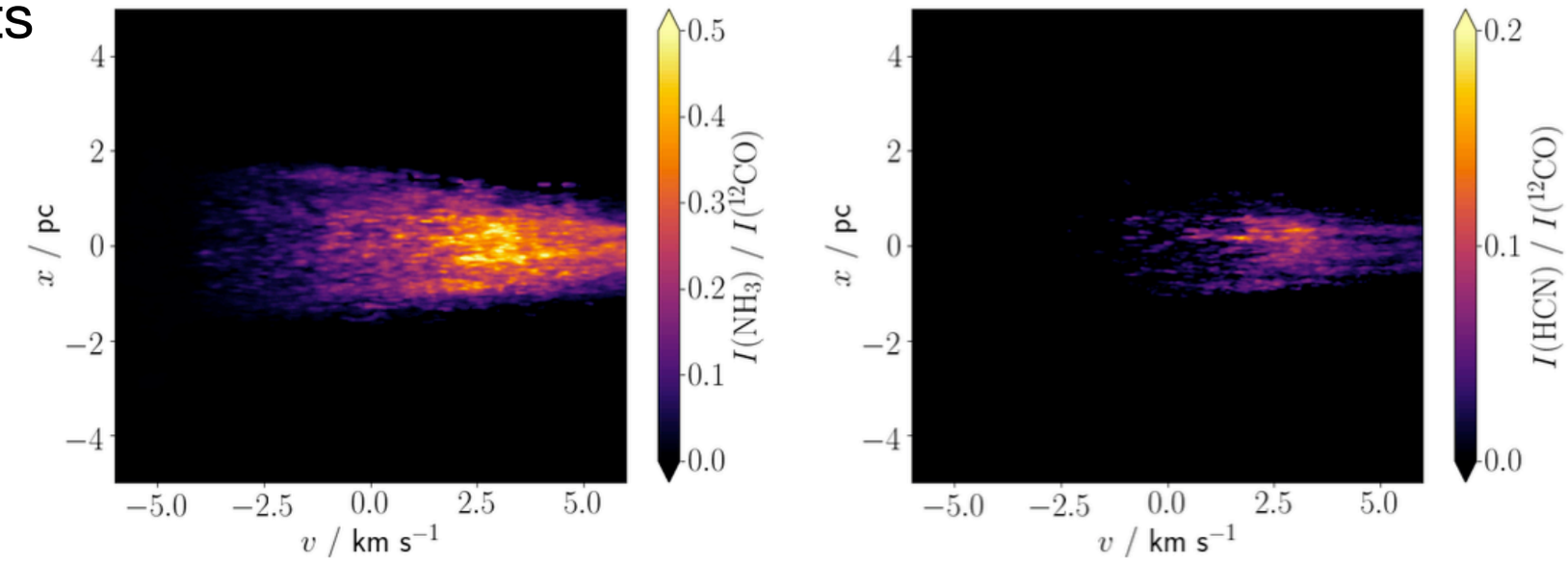


Chance-alignment

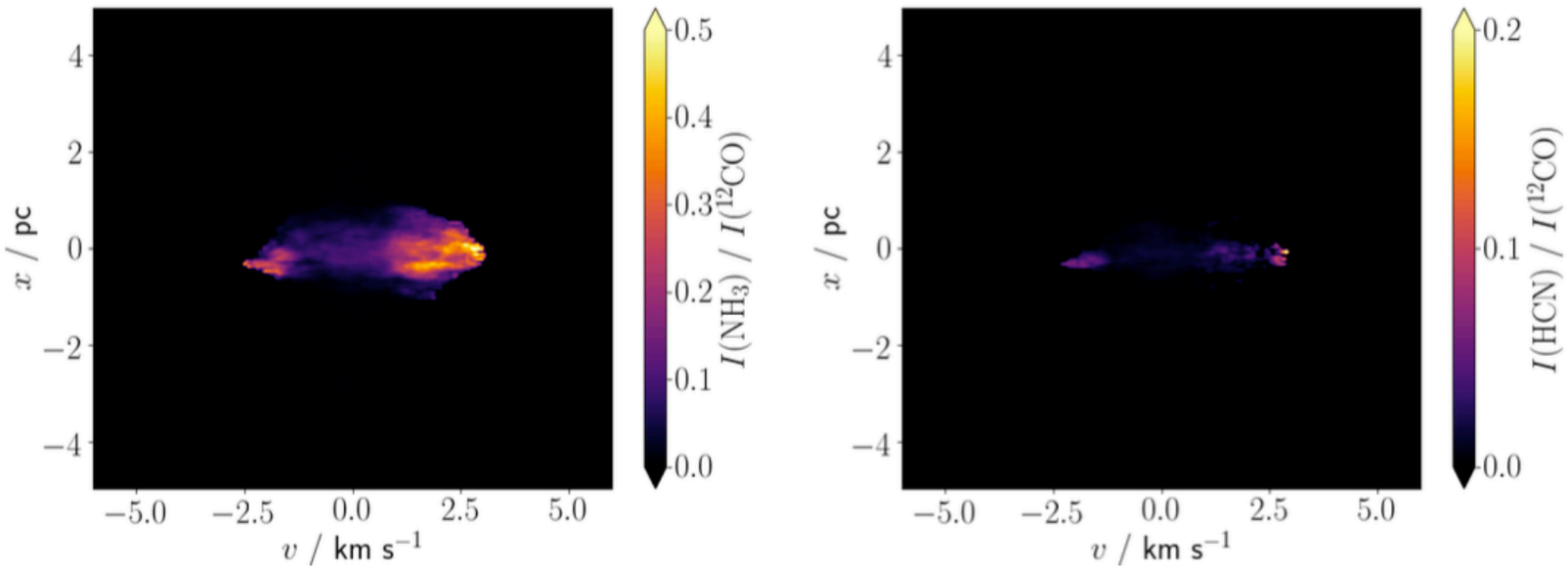


- Conclusion

  - Cloud-cloud collisionが起こっている場合、NH3, HCNの輝線はCOとは異なり圧縮層で強くなるため、これを利用して観測されたBridging featureが本当にcollision由来なものかどうか検証することが可能となるだろう

# 21. Characterization of dense Planck clumps observed with Herschel and SCUBA-2

Mannfors et al.


## ABSTRACT

*Context.* Although the basic processes of star formation (SF) are known, more research is needed on SF across multiple scales and environments. The Planck all-sky survey provided a large catalog of Galactic cold clouds and clumps that have been the target of several follow-up surveys.

*Aims.* We aim to characterize a diverse selection of dense, potentially star-forming cores, clumps, and clouds within the Milky Way in terms of their dust emission and SF activity.

*Methods.* We studied 53 fields that have been observed in the JCMT SCUBA-2 continuum survey SCOPE and have been mapped with *Herschel*. We estimated dust properties by fitting *Herschel* observations with modified blackbody functions, studied the relationship between dust temperature and dust opacity spectral index $\beta$, and estimated column densities. We extracted clumps from the SCUBA-2 850 $\mu$m maps with the FellWalker algorithm and examined their masses and sizes. Clumps are associated with young stellar objects found in several catalogs. We estimated the gravitational stability of the clumps with virial analysis. The clumps are categorized as unbound starless, prestellar, or protostellar.

*Results.* We find 529 dense clumps, typically with high column densities from $(0.3–4.8)\times10^{22}\,\mathrm{cm}^{-2}$, with a mean of $(1.5\pm0.04)\times10^{22}\,\mathrm{cm}^{-2}$, low temperatures ($T$ ~10 –20 K), and estimated submillimeter $\beta=1.7\pm0.1$. We detect a slight increase in opacity spectral index toward millimeter wavelengths. Masses of the sources range from 0.04 $\mathrm{M}_\odot$ to 4259 $\mathrm{M}_\odot$. Mass, linear size, and temperature are correlated with distance. Furthermore, the estimated gravitational stability is dependent on distance, and more distant clumps appear more virially bound. Finally, we present a catalog of properties of the clumps.

*Conclusions.* Our sources present a large array of SF regions, from high-latitude, nearby diffuse clouds to large SF complexes near the Galactic center. Analysis of these regions will continue with the addition of molecular line data, which will allow us to study the densest regions of the clumps in more detail.


**Key words.** Methods: observational – Stars: formation – ISM: clouds – ISM: dust, extinction – Infrared: ISM – ISM: general

# 23. A stellar mass dependence of structured disks: a possible link with exoplanet demographics

Van der Marel et al.

ABSTRACT

Gaps in protoplanetary disks have long been hailed as signposts of planet formation. However, a direct link between exoplanets and disks remains hard to identify. We present a large sample study of ALMA disk surveys of nearby star-forming regions to disentangle this connection. All disks are classified as either structured (transition, ring, extended) or non-structured (compact) disks. Although low-resolution observations may not identify large scale substructure, we assume that an extended disk must contain substructure from a dust evolution argument. A comparison across ages reveals that structured disks retain high dust masses up to at least 10 Myr, whereas the dust mass of compact, non-structured disks decreases over time. This can be understood if the dust mass evolves primarily by radial drift, unless drift is prevented by pressure bumps. We identify a stellar mass dependence of the fraction of structured disks. We propose a scenario linking this dependence with that of giant exoplanet occurrence rates. We show that there are enough exoplanets to account for the observed disk structures if transitional disks are created by exoplanets more massive than Jupiter, and ring disks by exoplanets more massive than Neptune, under the assumption that most of those planets eventually migrate inwards. On the other hand, the known anti-correlation between transiting super-Earths and stellar mass implies those planets must form in the disks without observed structure, consistent with formation through pebble accretion in drift-dominated disks. These findings support an evolutionary scenario where the early formation of giant planets determines the disk's dust evolution and its observational appearance.

*Keywords:* Protoplanetary disks - Stars: formation

# 24. Spectral index of synchrotron emission: insights from the diffuse and magnetised interstellar medium

Padovani et al.


## ABSTRACT

*Context.* The interpretation of Galactic synchrotron observations is complicated by the degeneracy between the strength of the magnetic field perpendicular to the line of sight (LOS), $B_\perp$, and the cosmic-ray electron (CRe) spectrum. Depending on the observing frequency, an energy-independent spectral energy slope $s$ for the CRe spectrum is usually assumed: $s = -2$ at frequencies below $\simeq$400 MHz and $s = -3$ at higher frequencies.

*Aims.* Motivated by the high angular and spectral resolution of current facilities such as the LOw Frequency ARray (LOFAR) and future telescopes such as the Square Kilometre Array (SKA), we aim to understand the consequences of taking into account the energy-dependent CRe spectral energy slope on the analysis of the spatial variations of the brightness temperature spectral index, $\beta$, and on the estimate of the average value of $B_\perp$ along the LOS.

*Methods.* We illustrate analytically and numerically the impact that different realisations of the CRe spectrum have on the interpretation of the spatial variation of $\beta$. We use two snapshots from 3D magnetohydrodynamic simulations as input for the magnetic field, with median magnetic field strength of $\simeq 4$ and $\simeq 20\,\mu$G, to study the variation of $\beta$ over a wide range of frequencies ($\simeq 0.1-10$ GHz).

*Results.* We find that the common assumption of an energy-independent $s$ is valid only in special cases. We show that for typical magnetic field strengths of the diffuse ISM ($\simeq$2–20 $\mu$G), at frequencies of 0.1–10 GHz, the electrons that are mainly responsible for the synchrotron emission have energies in the range $\simeq$100 MeV–50 GeV. This is the energy range where the spectral slope, $s$, of CRe has its greatest variation. We also show that the polarisation fraction can be much smaller than the maximum value of $\simeq 70\%$ because the orientation of $\mathbf{B}_\perp$ varies across the telescope's beam and along the LOS. Finally, we present a look-up plot that can be used to estimate the average value of $B_\perp$ along the LOS from a set of values of $\beta$ measured at different frequencies, for a given CRe spectrum.

*Conclusions.* In order to interpret the spatial variations of $\beta$ observed from centimetre to metre wavelengths across the Galaxy, the energy-dependent slope of the Galactic CRe spectrum in the energy range $\simeq$100 MeV–50 GeV must be taken into account.


**Key words.** ISM: cosmic rays – ISM: magnetic fields – ISM: clouds – ISM: structure – radio continuum: ISM – radiation mechanisms: non-thermal

# 26. Understanding the angular momentum evolution of T Tauri and Herbig Ae/Be stars

Pinzon et al.

ABSTRACT

We investigate a sample of 6 Herbig Ae/Be stars belonging to the Orion OB1 association, as well as 73 low mass objects, members of the $\sigma$ Orionis cluster, in order to explore the angular momentum evolution at early stages of evolution, and its possible connection with main-sequence Ap/Bp magnetic stars. Using FIES and HECTOCHELLE spectra, we obtain projected rotational velocities through two independent methods. Individual masses, radii, and ages were computed using evolutionary models, distance, and cluster extinction. Under the assumption that similar physical processes operate in both, T Tauri and Herbig Ae/Be stars, we construct snapshots of the protostar's rotation against mass during the first 10 Myr with the aid of a rotational model that includes a variable disc lifetime, changes in the stellar moment of inertia, a dipolar magnetic field with variable strength, and angular momentum loss through stellar winds powered by accretion. We use these snapshots, as well as the rotational data, to infer a plausible scenario for the angular momentum evolution. We find that magnetic field strengths of a few k$G$ at 3 Myr are required to match the rotational velocities of both groups of stars. Models with masses between 2-3 $M_{\odot}$ display larger angular momentum by a factor of $\sim 3$, in comparison to stars of similar spectral types on the main-sequence. Even though some quantitative estimates on this dramatic decrease with age, for Ap/Bp magnetic main-sequence stars are presented, the results obtained for the angular momentum evolution do not explain their low rotation.

*Keywords:* editorials, notices — miscellaneous — catalogs — surveys